Optimally designed potentials for control of electron-wave scattering in semiconductor nanodevices

Peter Gross, Viswanath Ramakrishna, Eduardo Vilallonga, and Herschel Rabitz
Department of Chemistry, Princeton University, Princeton, New Jersey 08544

Michael Littman
Department of Mechanical and Aerospace Engineering, Princeton University, Princeton, New Jersey 08544

Stephen A. Lyon and Mansour Shayegan
Department of Electrical Engineering, Princeton University, Princeton, New Jersey 08544
(Received 23 August 1993)

Control of plane-wave scattering is examined using designed potential structures in solid-state devices with dimensions of the electron coherence length. Reflection coefficients at specified incident electron energies are controlled by exploiting the quantum interference effects associated with the wavelike nature of the electrons through optimally designed manipulation of the solid-generated scattering potential. This work is motivated by the increasing ability to fabricate semiconductor structures with controlled layer thickness and lateral features, and here the goal is to demonstrate the degree of coherent electron control achievable through the employment of optimal design tools. We examine the case where the potential form is restricted to a fixed number of rectangular barriers. Here, the optimization of the design is performed with respect to the barrier width and spacings in order to achieve the desired reflection coefficients at one or more incident energies. We also examine the case where the potential is not restricted to any particular form, and here optimal control theory is employed to optimize the scattering potential form in order to achieve the desired reflection coefficients over a range of incident electron energies. The possibility of extending this work to controlling electron wave-packet structures is also discussed.

I. INTRODUCTION

With the introduction of sophisticated semiconductor epitaxial growth and fabrication techniques, it has become possible to create devices with dimensions on the order of the electron wavelength at energies of $\approx 1-100$ meV.[1,2] For semiconductor devices of this size, quantum transport is ballistic, i.e., the electrons travel without experiencing collisions and thus quantum-mechanical wave effects such as diffraction and refraction are observed. Indeed, the interference effects exhibited in nanoscale semiconductor devices are analogous to electromagnetic waves in conventional optical thin-film dielectric devices (see Ref. 3 and references cited therein). Examples of such devices include quantum dots, wires, and the two-dimensional electron gas in GaAs-$Al_xGa_{1-x}As$ heterostructures.[1,2] This technology allows one to observe and possibly exploit the wavelike properties of electrons and opens up the door to electronic devices which are not governed by diffusive transport (i.e., bulk properties such as current and voltage) but by the coherent wave-packet structure of the individual electrons. Ideally, in such devices each electron can be "encoded" with information through manipulation of the Fourier components of its wave function and then subsequently decoded elsewhere in the circuit, thus allowing for a vast increase in information-transfer capability over what is presently available.

The work presented here is a first step towards realizing the goal of electron wave-packet encoding and decoding. Here the physics is limited to plane-wave scattering, where the physical objective is to optimize the reflection coefficients at specified incident electron energies. Since an arbitrary wave packet $\psi_{\rm inc}(x,t)$ moving in one dimension x (here taken as incident from the left) can always be expanded in terms of its Fourier components, i.e., $\psi_{\rm inc}(x,t)=\int_0^\infty f(k)\exp[i(kx-\omega t)]dk$, this work is a prelude to designing potentials which act as energy "filters" to allow through only certain specified energy components of the incoming wave packet. Moreover, the scattering potential can alter the amplitude and phase of each Fourier component, thereby allowing one to produce a wide variety of wave-packet structures. In the Appendix we explore the question of the existence of a local spatial potential which will produce a desired wave packet from a given primitive wave packet, provided that there are no laboratory restrictions on the potential form. Such an analysis is necessary to discern the limitations of the type of endeavor which the present paper addresses. In particular, we will see that not every wave packet can be synthesized, although one could (in principle) come up with a list of final wave packets which can be synthesized from the given primitive wave packet (again, with no further laboratory restrictions). In all cases, successful manipulation of the wave packet will depend upon quantum interference effects.

To obtain a desired wave-packet structure, the potential in the solid-state device structure must be designed such that when an injected electron is scattered over this potential it provides the desired outgoing wave packet.

0163-1829/94/49(16)/11100(11)/$06.00

The potential might be imposed laterally, e.g., with a one-dimensional grating potential constructed by electron-beam lithography, or vertically, as in a superlattice fabricated using epitaxial growth techniques. The required potential structure will likely not be obvious and will possibly be counterintuitive. Therefore, it will be necessary to employ various mathematical design and optimization procedures including optimal control theory, which have been used extensively in the past few years as a means for designing laser fields to produce desired molecular objectives such as cleavage of a particular chemical bond in a triatomic system.[4] Optimal control theory has proven quite successful because it allows for a wide latitude of physical goals including laboratory constraints and robustness concerns. In this work, optimal control theory is used to design the potential of the solid-state device structure. This is a fundamentally different application from the aforementioned studies involving molecular objectives, in that here we are actually manipulating the system Hamiltonian (the potential) rather than some external forcing function (the electric field) which, through the molecular dipole function, can couple with the internal dynamics of the system but is not a part of the molecular field-free (i.e., system) Hamiltonian.

The balance of the paper is as follows. Section II presents the optimization algorithm and results for electron plane-wave scattering where the potential form is restricted to a series of rectangular barriers. In this case only the widths and spacings of the barriers are optimized in order to drive the reflection coefficient at one or several incident energies to a specified set of objective values. In Sec. III optimization of the reflection coefficients both at a single energy and over a continuous range of energies is done using a "free-floating" potential, i.e., one that is not restricted to any particular form. Here, optimal control theory is employed to design the scattering potential. The physical interpretation of the optimal potential and the manifestation of quantum interference effects are discussed. Conclusions and future extensions are briefly discussed in Sec. IV.

II. POTENTIAL-BARRIER OPTIMIZATION

Here we explore the possibility of obtaining a desired reflection coefficient $R(E)$ at one or more incident electron plane-wave energies through manipulation of the spacing and widths of a series of rectangular potential barriers. The scattering potential $V(x)$ is restricted to a fixed number of barriers (five) of height $V_B=0.005$ eV above the ground potential V_0, taken to be 0.0 eV. Only the positions of the barrier edges $x_2,x_3,\ldots,x_9$ are optimized; the total length of the potential, $x_{10}-x_1$, is fixed. For the initial guess potential we take the width used in the optimization procedure (see below) of all five barriers to be 4000 Å and the spacing between barriers 6000 Å (see Fig. 1).

To compute the reflection coefficient $R(E)$ (within the effective-mass approximation) we must solve the time-independent Schrödinger equation:

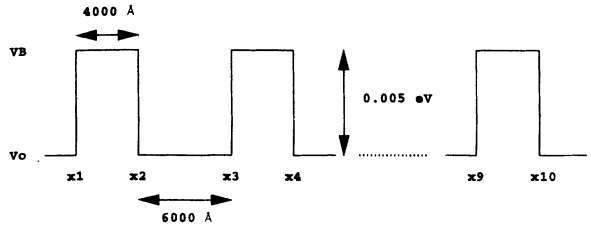

FIG. 1. Initial guess potential $V^{(i=0)}(x)$ consisting of five equally spaced barriers for the potential-barrier optimization.

$$\frac{-\hbar^2}{2m}\frac{d^2\psi}{dx^2}+[V(x)-E]\psi(x)=0\ , \tag{1}$$

where $m=0.067m_e$ is the effective mass of the electron and E is the incident energy of the plane-wave electron. We proceed in the standard manner[5] by first solving Eq. (1) analytically for each piecewise constant potential, i.e.,

$$\begin{aligned}
&\psi(x)=A_0\exp(ik_0x)+B_0\exp(-ik_0x)\quad (x<x_1)\ ,\\
&\psi(x)=A_1\exp(ik_Bx)+B_1\exp(-ik_Bx)\quad (x_1<x<x_2)\ ,\\
&\qquad\vdots\\
&\psi(x)=A_{10}\exp(ik_0x)+B_{10}\exp(-ik_0x)\quad (x>x_{10})\ ,
\end{aligned} \tag{2}$$

where $k_0=\sqrt{2m(E-V_0)}/\hbar$, $k_B=\sqrt{2m(E-V_B)}/\hbar$, ($V_B=0.005$ eV), and $B_{10}=0.0$, since the electron wave is assumed to be incident from the left. By matching the wave function and its slope at the potential discontinuities, we can solve for the A_n and B_n coefficients and write

$$\begin{bmatrix}A_0\\B_0\end{bmatrix}=\mathbf{S}(x_1)\mathbf{S}(x_2)\ldots\mathbf{S}(x_{10})\begin{bmatrix}A_{10}\\0\end{bmatrix}=\mathbf{S}^P\begin{bmatrix}A_{10}\\0\end{bmatrix}\ , \tag{3}$$

where $\mathbf{S}^P$ is the 2×2 transfer matrix connecting the incident and reflected waves with the transmitted wave. The reflection coefficient is defined as the ratio of the reflected wave to the incident wave:

$$R(E)=\frac{|B_0|^2}{|A_0|^2}=\frac{|S_{21}^P|^2}{|S_{11}^P|^2}\ . \tag{4}$$

To perform the optimization, a cost functional is constructed whose minimization corresponds to obtaining the desired physical goals, i.e., the desired reflection coefficients at M specified energies:

$$J=\sum_{m=1}^{M}[R'(E_m)-R(E_m)]^2\ , \tag{5}$$

where $R'(E_m)$ and $R(E_m)$ are the objective and actual reflection coefficients, respectively, at incident energy E_m. To minimize J we employ a gradient-based steepest-descent procedure which iteratively optimizes the parameters $x_2,x_3,\ldots,x_9$:

$$x_n^{(i+1)}=x_n^{(i)}-\alpha\frac{\partial J}{\partial x_n^{(i)}}\ , \tag{6}$$

where i is the iteration counter and α is a small, positive constant. The explicit form of the gradients is

$$\frac{\partial J}{\partial x_n} = -2 \sum_{m=1}^{M} [R'(E_m) - R(E_m)] \frac{\partial}{\partial x_n} \frac{|S_{21}^P|^2}{|S_{11}^P|^2} , \quad (7)$$

where the derivative of the term $|S_{11}^P|^2/|S_{11}^P|^2$ requires the derivative of the 2×2 transfer matrix $\mathbf{S}^P$, i.e.,

$$\frac{\partial}{\partial x_n}\mathbf{S}^P = \mathbf{S}(x_1)\cdots\frac{\partial}{\partial x_n}\mathbf{S}(x_n)\cdots\mathbf{S}(x_{10}) . \quad (8)$$

We first examine the optimization of $R(E)$ at a single energy. The goal in this case is to maximize the reflection coefficient at $E_1 = 0.01$ eV and so we set $R'(E_1) = 1.0$ in Eq. (5). The value of $R(E_1)$ using the initial guess potential $V^{(i=0)}(x)$ shown in Fig. 1 is 0.0057, as indicated by the far right arrow in Fig. 2(a) which displays $R(E)$ over a range of energies from 0.0075 to 0.0105 eV. Note that the de Broglie wavelength of the electron in this range is 547–462 Å and the complicated structure in Fig. 2(a) is due to the resonances created by the potential. The optimal potential-barrier parameters are shown in Table I. (column 2); note that they differ by a rather small amount (<150 Å) from their initial guess values relative to the barrier widths (4000 Å). The change in $R(E)$, however, is dramatic, as seen in Fig. 2(b), which plots the reflection coefficient vs energy using the optimized potential-barrier parameters. Note in particular the arrow in Fig. 2(b), which indicates the reflection coefficient at the target energy $E_1 = 0.01$ eV which now is 0.73. By comparing Figs. 2(a) and 2(b), we see that the effect of the optimization was more or less to "shift" the reflection peaks, or resonances, such that a large reflection occurs at $E = 0.01$ eV using the optimal barrier parameters. This limited "shifting" also implies that the closer the target energy E_1 is to the barrier height V_B, the higher the reflection coefficient one can attain. This is to be expected since the reflection peaks become more pronounced at lower energies.

Next we present results for a more interesting case where the goal now is to reach specified reflection-coefficient values simultaneously at *three* incident energies: $E_1 = 0.008$, $E_2 = 0.009$, and $E_3 = 0.010$ eV. The objective reflection coefficients at these energies are $R'(E_1) = 0.3$, $R'(E_2) = 0.4$, and $R'(E_3) = 0.2$. The reflection coefficients at target energies E_1, E_2, and E_3 using the same initial guess potential as in the previous

TABLE I. Barrier parameters for initial guess potential (1), the optimal potential where the objective reflection coefficient at one energy is specified (2), and the optimal potential where the objective reflection coefficient at three energies is specified (3) (in Angstroms).

Position	(1) (Å)	(2) (Å)	(3) (Å)
x_1 (fixed)	0.0	0.0	0.0
x_2 (variable)	4000.0	3953.5	3988.2
x_3 (variable)	10000.0	9976.2	10015.9
x_4 (variable)	14000.0	13865.3	14055.1
x_5 (variable)	20000.0	19887.9	19965.3
x_6 (variable)	24000.0	24112.1	24034.7
x_7 (variable)	30000.0	30134.7	29944.9
x_8 (variable)	34000.0	34023.8	33984.1
x_9 (variable)	40000.0	40046.5	40011.8
x_{10} (fixed)	44000.0	44000.0	44000.0

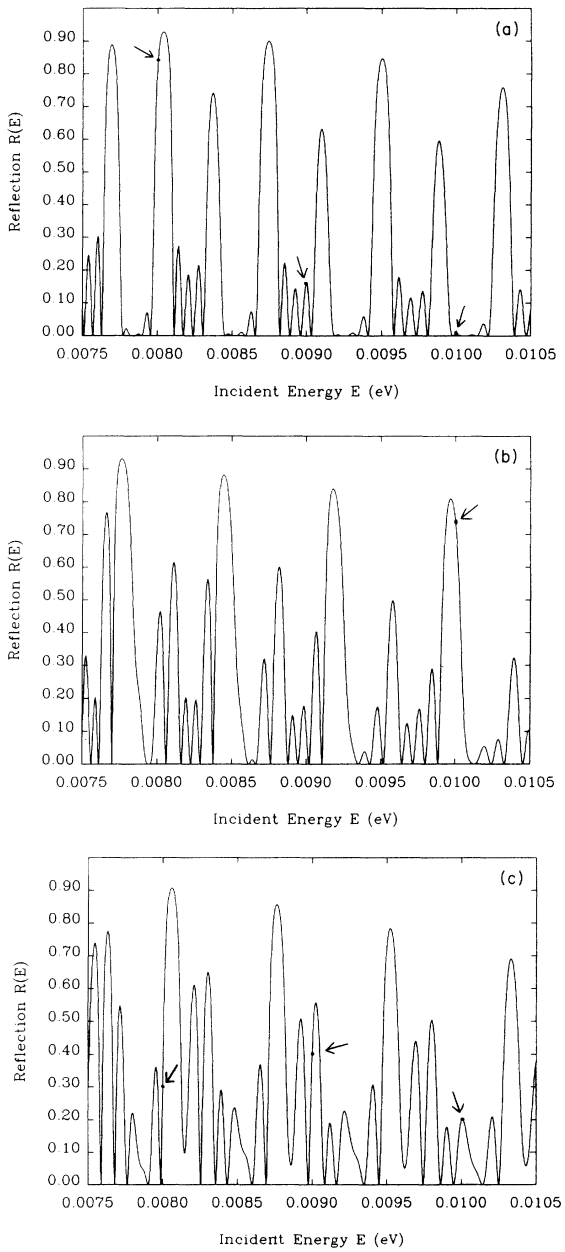

FIG. 2. Reflection coefficient vs incident energy using the initial guess potential shown in Fig. 1. The arrows indicate the target energies 0.008, 0.009, and 0.01 eV at which the reflection coefficient $R(E)$ is to be optimized. (b) Same as (a) except using the optimal potential-barrier parameters designed for maximizing the reflection coefficient at 0.01 eV. The achieved value (0.73) is indicated by the arrow. (c) Same as (a) except using the optimal potential designed for achieving reflection coefficients of 0.3, 0.4, and 0.2 at target energies 0.008, 0.009, and 0.01 eV. The achieved values match their objective values to within 0.1% and are indicated by the three arrows.

case are 0.83, 0.16, and 0.0057, respectively, as indicated by the three arrows in Fig. 2(a). As noted in the Introduction, this multiple-reflection-coefficient objective can be viewed as a first step towards the ultimate goal of wave-packet encoding, in that we may think of the target energies here as corresponding to three Fourier components of the incident wave packet. Controlling the reflection coefficient of these energies is analogous to controlling the corresponding Fourier component amplitudes of a wave packet, but there is no provision here for controlling their phases since the reflection coefficient is the *absolute value* squared of the incident wave over the reflected wave.

The optimized barrier parameters are shown in column 3 of Table I. Again, as in the previous case, the change in barrier parameters from their initial guess values is very small compared to the barrier widths. Figure 2(c) shows $R(E)$ using the optimal potential; the reflection coefficients for the target energies indicated by the three arrows all match the goals to within 0.1% of the objective values. Although the potential optimization proved very adequate in this case, the solution is evidently somewhat unstable, given that the optimized reflection coefficients at E_1 and E_2 reside on the sides of the reflection peaks in Fig. 2(c), thereby indicating that a small error in the barrier parameters would result in very different reflection coefficients at these energies. Significant uncertainties in the incident electron energies may also lead to substantially different reflection-coefficient values than one expects. To make the solution more stable, we would need to resort to some form of robust control, which will be examined in future work.

Finally, we note that the sharp edges of the rectangular barriers shown in Fig. 1 are responsible for the quantum interference effects, which manifest themselves here by the complex structure of the reflection coefficient over a range of incident energies in both the initial guess and optimized potentials. In practice, however, it will be very difficult to construct heterostructure devices which possess abrupt lateral potentials. Rather, the edges of the potential barriers in such structures will have a finite width, of the order of the distance from the surface to the two-dimensional electron gas. The smoother the edges relative to the electron de Broglie wavelength, the less the "diffraction" of the electron waves, thereby resulting in damping of interference patterns. This is demonstrated in Fig. 3, which presents scattering calculations using the same general potential form as that shown in Fig. 1, except that here the barriers are trapezoids, i.e., the width at the top of the barriers is 4000 Å but the width at the bottom is 4400 Å. As expected, the reflection pattern here is less pronounced compared to that with the rectangular barriers in Fig. 2(a), and thus optimization of trapezoidal widths to maximize the reflection coefficient at a particular incident energy (not shown here) was not as successful as the rectangular-barrier case. However, we stress that in the case of vertical structures it is easier to fabricate sharp-edged potentials. One must keep in mind that in the case of vertical structures higher energies and shorter length scales (of structures) are more relevant.

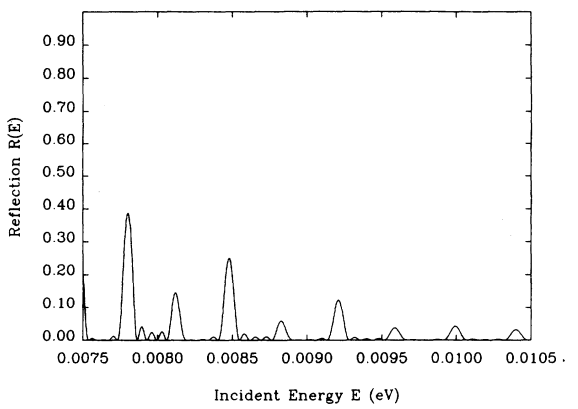

FIG. 3. Reflection coefficient vs incident energy using five equally spaced trapezoidal barriers. Note that the reflection peaks are much less intense than in the case using rectangular barriers shown in Fig. 2(a).

III. FREE-FLOATING POTENTIAL DESIGN OPTIMIZATION

Now we extend the same problem of optimization of the reflection coefficients by allowing the entire potential function to be optimized. Here $V(x)$ is no longer restricted to a particular form as in Sec. II where it was composed of five rectangular barriers. Since we are now optimizing a *function* rather than a small set of parameters, optimal control theory is employed to design the potential. As one might intuitively expect, the freedom to modify the entire potential provides one with better control.

Before describing the optimal control formalism used in this problem, we outline the method used to calculate the reflection coefficients $R(E)$ for an arbitrary potential form such as that shown in Fig. 4. First, it is assumed that the incoming electron waves are incident from the left of the scattering potential $V(x)$. For the asymptotic region $x < x_l$, the solution of Schrödinger's equation is (at a given incident energy E)

$$\psi(x) = A \exp(ik_0 x) + B \exp(-ik_0 x) , \tag{9}$$

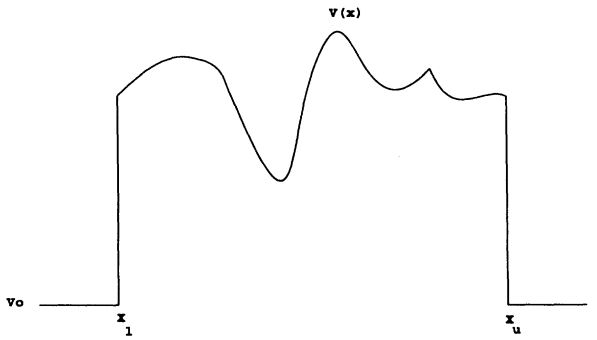

FIG. 4. Schematic of the "free-floating" potential used to optimize $R(E)$ with the optimal control algorithm. Only the potential in the region $x \in [x_l, x_u]$ is optimized; for $x < x_l$ and $x > x_u$ the potential is fixed at 0.0 eV.

where $k_0=\sqrt{2m(E-V_0)}/\hbar$, and $V_0=0.0$ eV is the constant ground potential, i.e., the potential outside the range $x\in[x_l,x_u]$. The constants A and B are obtained, as usual, by equating the values at x_l of the wave function and its derivative to those of the function on the right-hand side of Eq. (9). The reflection coefficient is the ratio of the probability amplitude of the reflected to the incident wave:

$$R(E)=\frac{|B|^2}{|A|^2} . \tag{10}$$

Computation of $R(E)$ requires the knowledge of $\psi(x_l)$ and $\psi'(x_l)$ at incident energy E; these are computed by numerically integrating the time-independent Schrödinger equation "backwards" from the upper boundary x_u to x_l with the Numerov algorithm.[6] Since we are solving a second-order differential equation, two boundary conditions, $\psi(x_u)$ and $\psi'(x_u)$ must be specified. These are determined by the solution of the wave function in the asymptotic region $x>x_u$:

$$\psi(x)=F\exp(ik_0x) . \tag{11}$$

Note the absence of the $\exp(-ik_0x)$ term in Eq. (11), since the incoming electron waves are assumed to be incident from the left. The initial conditions $\psi(x_u)$ and $\psi'(x_u)$ must, of course, be consistent with the asymptotic solution in Eq. (11). The (complex) value for F is completely arbitrary for the purposes of computing the reflection coefficient. In practice, we chose $F=1.0$.

We now turn to the optimization problem at hand. First, a cost functional whose minimization corresponds to achieving the desired physical goal of plane-wave reflection over a *continuous* range of energies is constructed:

$$J=\int_{E_l}^{E_u} dE\, W(E)[R'(E)-R(E)]^2 , \tag{12}$$

where $R'(E)$ and $R(E)$ are the objective and actual reflection coefficients defined previously, E_l and E_u are the lower and upper bounds of the incident electron energy for which the reflection coefficients are to be optimized, and $W(E)$ is a weighting function. The minimization of J is constrained by the time-independent Schrödinger equation,

$$\psi''(x;E)+b(x,E)\psi(x;E)=0 , \tag{13}$$

where $b(x,E)=-(2m/\hbar^2)[V(x)-E]$. Following the general quantum-mechanical optimal control formulation,[7] an unconstrained objective functional is formed via Lagrange multiplier function $\lambda(x;E)$:

$$\bar{J}=J-\left[\int_{E_l}^{E_u} dE\int_{x_l}^{x_u} dx\ \lambda(x;E)[\psi''(x;E)+b(x,E)\psi(x;E)]+\text{c.c.}\right] , \tag{14}$$

where c.c. denotes complex conjugate and x_l, x_u are the lower and upper boundaries of the spatial region where the potential is to be modified, as shown in Fig. 4.

Now an extremum (minimum) is found when an arbitrary first-order variation of $\bar{J}$ with respect to the $\lambda(x;E)$, $\lambda^*(x;E)$, $\psi(x;E)$, $\psi^*(x;E)$, and $V(x)$ are zero, i.e.,

$$\begin{aligned}\delta\bar{J}&=\bar{J}[\lambda+\delta\lambda,\lambda^*+\delta\lambda^*,\psi+\delta\psi,\psi^*+\delta\psi^*,V+\delta V]\\&\quad-\bar{J}[\lambda,\lambda^*,\psi,\psi^*,V]\\&=0 .\end{aligned} \tag{15}$$

For arbitrary variations in λ and λ^*, $\delta\bar{J}$ is zero since $\delta\bar{J}/\delta\lambda=\delta\bar{J}/\delta\lambda^*=0$, because Schrödinger's equation (13) is satisfied by construction. The Lagrange multipliers can be chosen such that the variation of $\bar{J}$ with respect to ψ and ψ^* is zero. Integrating the term $\lambda(x;e)\psi''(x;E)$ in Eq. (14) and its complex conjugate by parts twice gives

$$\bar{J}=J-\left[\int_{E_l}^{E_u} dE\left\{\psi'(x_u;E)\lambda(x_u;E)-\psi(x_u;E)\lambda'(x_u;E)+\psi(x_l;E)\lambda'(x_l;E)-\psi'(x_l;E)\lambda(x_l;E)+\int_{x_l}^{x_u} dx[\psi(x;E)\lambda''(x;E)+\lambda(x;E)b(x,E)\psi(x;E)]\right\}+\text{c.c.}\right] . \tag{16}$$

For the first-order variation of $\bar{J}$ with respect to $\psi(x;E)$ and $\psi'(x;E)$ to be zero, i.e., $\delta\bar{J}/\delta\psi(x;E)=\delta\bar{J}/\delta\psi'(x;E)=0$, the Lagrange multiplier functions must satisfy the differential (Schrödinger's) equation

$$\lambda''(x;E)+b(x,E)\lambda(x;E)=0 , \tag{17}$$

with the boundary conditions

$$\lambda(x_l;E)=2W(E)[R'(E)-R(E)]\frac{\partial R(E)}{\partial\psi'(x_l;E)} , \tag{18a}$$

$$\lambda'(x_l;E)=-2W(E)[R'(E)-R(E)]\frac{\partial R(E)}{\partial\psi(x_l;E)} , \tag{18b}$$

and similarly for choosing $\lambda^*(x;E)$ such that the variation of $\bar{J}$ with respect to $\psi^*(x;E)$ and $\psi'^*(x;E)$ is zero. Note that in deriving Eqs. (17) and (18) we have assumed that $\delta\psi(x_u;E)=\delta\psi'(x_u;E)=0$; this is true since $\psi(x_u;E),\psi'(x_u;E)$ (and their complex conjugates) are fixed by the boundary conditions on them derived from Eq. (9). [In practice, in order to prevent instabilities in the Numerov algorithm, it was necessary to scale the boundary conditions $\lambda(x_l;E)$ and $\lambda'(x_l;E)$ by $\approx10^{-5}$]. The explicit forms of the derivatives in Eq. (18) are

$$\frac{\partial R(E)}{\partial \psi'(x_l;E)} = \frac{i[k_0\psi'^*(x_l;E) - i\psi^*(x_l;E)]|A|^2 + i[k_0\psi^*(x_l;E) + i\psi'^*(x_l;E)]|B|^2}{|A|^4} , \tag{19a}$$

$$\frac{\partial R(E)}{\partial \psi(x_l;E)} = \frac{[k_0[k_0\psi^*(x_l;E) - i\psi'^*(x_l;E)]|A|^2 - k_0[k_0\psi^*(x_l;E) + i\psi'^*(x_l;E)]|B|^2}{|A|^4} . \tag{19b}$$

Finally at a minimum of $\bar{J}$ we require that the variation of $\bar{J}$ with respect to the potential $V(x)$ be zero, which leads to the condition

$$\frac{\delta \bar{J}}{\delta V(x)} = \frac{\delta \bar{J}}{\delta b(x,E)} \frac{\partial b(x,E)}{\partial V(x)} = \frac{4m}{\hbar^2} \int_{E_l}^{E_u} dE \, \mathrm{Re}\{\lambda(x;E)\psi(x;E)\} = 0 . \tag{20}$$

Now Eqs. (20), (17), and (13) form a set of coupled equations which must be solved iteratively. The algorithm employed in this work is as follows.

(1) Choose an initial guess potential $V^{(i=0)}(x)$ where $x \in [x_l, x_u]$.

(2) Set up the boundary conditions $\psi(x_u;E)$ and $\psi'(x_u;E)$ and integrate $\psi(x;E)$ backwards from x_u to x_l via Eq. (13).

(3) Set up the boundary conditions $\lambda(x_l;E)$ and $\lambda'(x_l;E)$ from Eq. (18) and integrate $\lambda(x;E)$ forwards form x_l to x_u via Eq. (17).

(4) Repeat steps (2) and (3) for all (discretized) incident energies in the range $E \in [E_l, E_u]$ and compute the gradient $\delta \bar{J}/\delta V(x)$ from the integral expression Eq. (20).

(5) Update the potential using the steepest-descent method:

$$V^{(i+1)}(x) = V^{(i)}(x) - \alpha \frac{\delta \bar{J}}{\delta V^{(i)}(x)} , \tag{21}$$

where α is a small, positive constant.

(6) Repeat steps (2)–(5) until a convergence criterion is met, i.e., $J[V^{(i+1)}(x)] - J[V^{(i)}(x)] < \gamma$, where γ is a small, positive number.

In the first optimization example, we seek to maximize the reflection coefficient at a single energy, $\tilde{E} = 0.01$ eV. Thus we set $W(E) = \delta(E - \tilde{E})$ and $R'(\tilde{E}) = 1.0$ in Eq. (15). The initial guess potential is assumed to be a constant (0.005 eV) with a length of $x_u - x_l = 8188$ Å. The potential outside this region is fixed at 0.0 eV. An upper bound (0.007 eV) was imposed on the height of $V(x)$ during the optimization in order to prevent it from becoming too large; this was necessary because any potential form with a height significantly greater than the target incident energy $\tilde{E}$ would result in the required high reflectivity. The optimal potential is shown in Fig. 5(a) and a plot of $R(E)$ using this potential over the range $0.008 < E < 0.012$ eV is shown in Fig. 5(b). Note that the objective $R(\tilde{E}) = 1.0$ is clearly reached, and that the optimal solution appears to be "robust" in the sense that $R(E) \approx 1.0$ over a fairly wide range about the target energy 0.01 eV.

The optimal potential in Fig. 5(a) is essentially a cosine wave with a mean energy of the initial guess potential, 0.005 eV. The important point to note about this oscillatory potential is that its "wavelength" is 335 Å, exactly one-half of the de Broglie wavelength of an electron at an incident energy of 0.01 eV passing over a constant potential barrier of 0.005 eV. This form can be interpreted in the following way. The general solution of Schrödinger's equation, assuming a constant potential, is a linear combination of the degenerate eigenfunctions $\psi(x) = A\exp(ikx) + B\exp(-ikx)$, where $k = \sqrt{2m(E - V_0)}/\hbar$ and $E = 0.01$ eV and $V_0 = 0.005$ eV in this case. If we write the optimal potential as $V(x) = V_0 + V\cos(k'x)$, then $V\cos(k'x)$ can be considered as the potential perturbation. The degenerate eigenfunctions $\exp(ikx)$ and $\exp(-ikx)$ of the unperturbed potential V_0 Hamiltonian are therefore the most natural choice for the basis functions for determining the

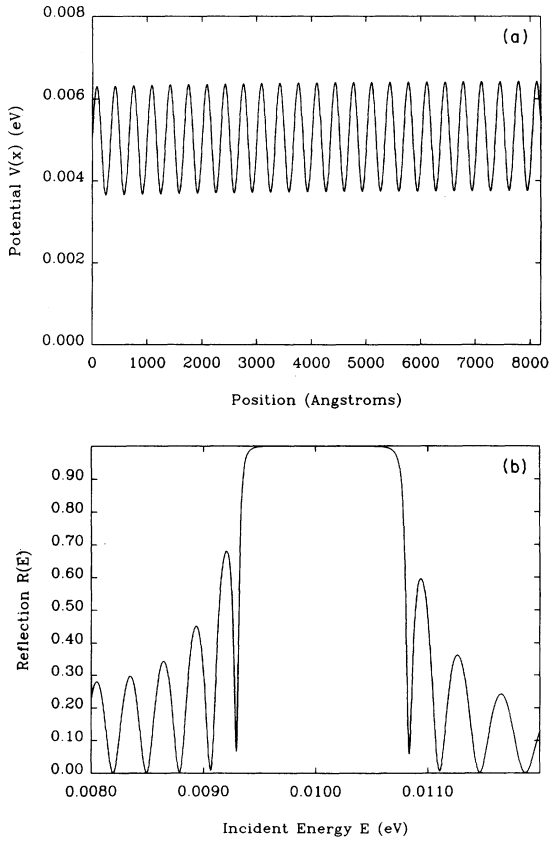

FIG. 5. (a) Optimal potential for maximizing $R(E)$ at a single incident energy $E = 0.01$ eV. The characteristic "wavelength" of the oscillatory potential structure is exactly one-half of the de Broglie wavelength of an electron with incident energy 0.01 eV passing over a constant potential region of 0.005 eV. (b) Reflection coefficient vs incident energy using the optimal potential shown in (a).

(first-order) wave functions of the full potential. Now, in a periodic potential, the eigenfunctions of the Hamiltonian must satisfy Bloch's theorem[8] $\psi_k(x)=u_k(x)\exp(ikx)$, where $u_k(x)$ possesses the same periodicity as the potential $V(x)$. If we write $\psi(x)$ as $[A+B\exp(-2ikx)]\exp(ikx)$, we see that $u_k(x)=A+B\exp(-2ikx)$, which oscillates with the same frequency as the optimal potential shown in Fig. 5(a) where $k'=2k$. This suggests that maximum control is obtained when the eigenfunctions (to first order) of the Hamiltonian with the optimal potential possess the same periodicity as the eigenfunctions of the Hamiltonian with the unperturbed (initial guess) potential. Apparently, the control algorithm employed finds an optimal potential such that the eigenfunctions are closely related to those corresponding to the initial guess constant potential.

This similarity between the optimal and initial guess potentials is indicative of the particular control algorithm employed in this work. Here, the algorithm relies on a gradient-based optimization procedure and is therefore only capable of finding a solution corresponding to a local minimum of the objective functional. Also, due to the local nature of gradient-based methods, the solution is heavily dependent upon the initial guess, so it is not surprising that there are similarities between the initial guess and optimal potentials as described above. Indeed, as was noted in the previous section where the potential was restricted to a fixed number of rectangular barriers, the optimal potential does not wander too far away from the initial guess potential due to the local nature of the optimization algorithm. It will be valuable to explore the use of more global algorithms which may reveal other good quality design solutions.

It is also worth noting that the perturbation $V\cos(k'x)$ causes a splitting (to first order) of the degenerate states proportional to $V\int dx\cos(k'x)\cos(kx)$; this integral is a maximum when $k'=2k$. Apparently, maximum control is obtained when the energy splitting is the greatest. This is somewhat analogous to the nearly-free-electron model used to explain the origin of the energy gap in infinite unbounded crystals,[8] in which the potential is proportional to $\cos(2\pi x/a)$, where a is the lattice constant and the stationary (standing-wave) states split by this perturbation are $2\cos(\pi x/a)$ and $2i\sin(\pi x/a)$. The only difference in our case is that although the reflection is (nearly) 1.0 transmission must be (nearly) zero. This means that we must have $F/A\approx 0.0$, where F is the coefficient of the outgoing plane wave [see Eq. (11)]. Thus the amplitude of the calculated wave function, $|\psi(x)|^2$, using the optimal potential (not shown here) behaves as $\sin^2(kx)$ as in the nearly-free-electron model, but here increases in amplitude exponentially from x_u to x_l in order to achieve (nearly) zero transmission. (At a surface or at a junction, solutions with complex wave vectors can exist, and then the analogy between the results presented here and the origin of the energy gap is more exact.)

Finally, regarding the optimal potential in Fig. 5(a) we note that there is a strong similarity between this potential form and quarter-wave stacks used in bandpass filter designs in optics when broadband reflectance about a particular wavelength is desired. A quarter-wave stack is composed of alternating layers of high- and low-refractive-index materials, and the thickness of each layer is one-quarter of the wavelength that is to be reflected. When light of the desired wavelength passes through the stack, alternate reflections are phase shifted by 180° due to transmittance from low- to high-refractive-index ma-

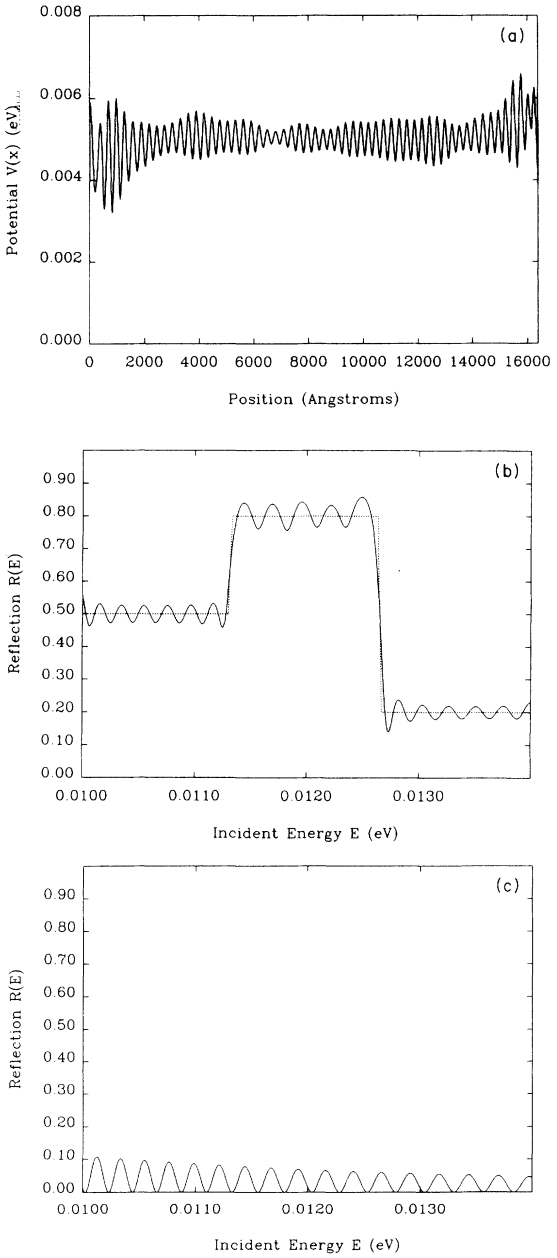

FIG. 6. (a) Optimal potential for achieving objective reflection coefficients over a range of energies: $R'(E)=0.5$ for $0.01<E<0.011\,33$ eV, $R'(E)=0.8$ for $0.011\,33<E<0.012\,66$ eV, and $R'(E)=0.2$ for $0.012\,66<E<0.014$ eV. (b) Reflection coefficient vs incident energy using the optimal potential shown in (a) (solid line) superimposed on the objective reflection coefficients $R'(E)$ (dotted line). (c) Reflection coefficient vs incident energy using the initial guess potential $V^{(i=0)}(x)=0.005$ eV for the "free-floating" results.

terials. These phase shifts are exactly canceled by phase shifts caused by the path difference between alternating reflecting surfaces. Thus the reflection wave fronts are exactly in phase and produce a reflection maximum. In the optimal potential shown in Fig. 5(a), each half "wavelength," equivalent to one-quarter of the incident electron de Broglie wavelength, is a layer in the quarter-wave stack. The alternating peaks and troughs of the potential correspond to alternating high- and low-refractive-index materials. The resulting broadband reflection pattern shown in Fig. 5(b) is qualitatively very similar to a typical optical reflectance curve produced by a quarter-wave stack.

We now turn to the more general problem of optimizing the reflection coefficient $R(E)$ over the range of energies $E \in [E_l, E_u] = [0.01, 0.014]$ eV. Here $W(E) = 1.0$ for all E and the objective reflection coefficient function is $R'(E) = 0.5$ for $0.01 < E < 0.011\,33$ eV, $R'(E) = 0.8$ for $0.011\,33 < E < 0.012\,66$ eV, and $R'(E) = 0.2$ for $0.012\,66 < E < 0.014$ eV. Again, the initial guess potential is a constant (0.005 eV), but here the spatial range $x_u - x_l$ over which the potential is optimized is 16 380 Å. Also, in this case there is no upper bound put on the potential as in the previous case. Figure 6(a) displays the optimal potential and Fig. 6(b) plots $R(E)$ using this potential (solid line) superimposed on the objective reflection $R'(E)$ (dotted line). Note that the agreement between the achieved and the goal reflection coefficients

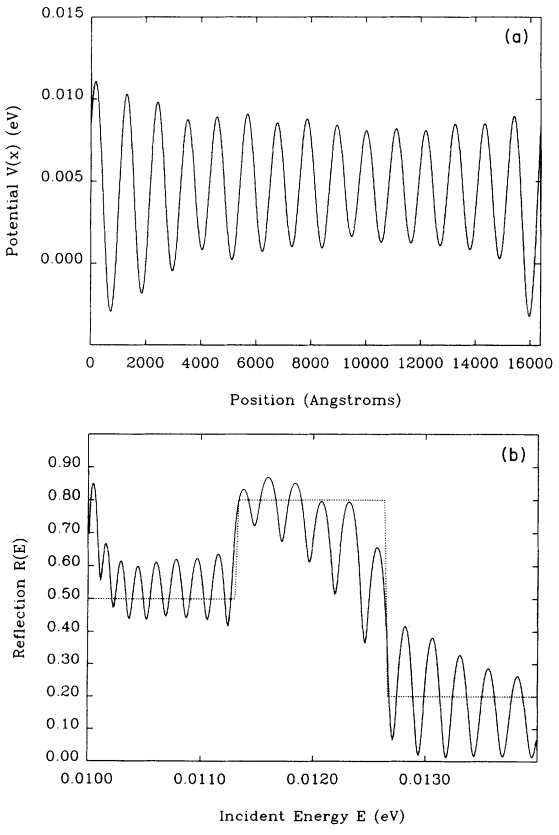

FIG. 7. (a) Optimal potential for achieving the same objective reflection coefficients as in Fig. 6(b) except here the "bandwidth" of the optimal potential is restricted such that the smallest possible "wavelength" component the potential may contain is 1000 Å. (b) Reflection coefficient vs incident energy using the optimal potential shown in (a) (solid line) superimposed on the objective reflection coefficients $R'(E)$ (dotted line).

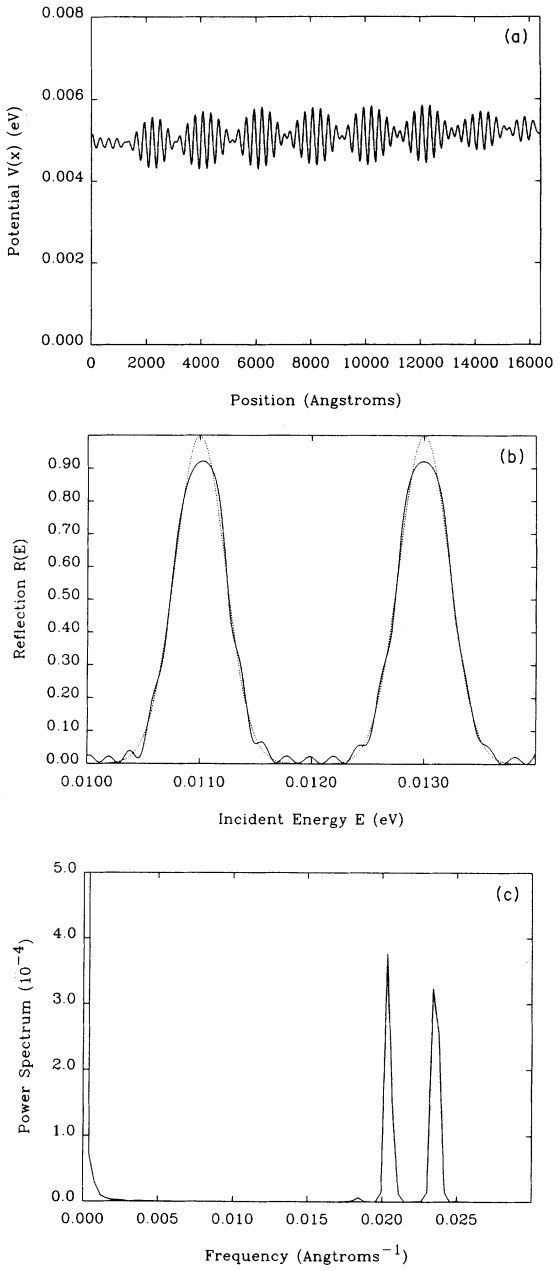

FIG. 8. (a) Optimal potential for achieving objective reflection coefficients which represent two narrow Gaussians centered at 0.011 and 0.013 eV. (b) Reflection coefficient vs incident energy using the optimal potential shown in (a) (solid line) superimposed on the objective reflection coefficients $R'(E)$ (dotted line). (c) "Power spectrum" of the optimal potential shown in (a). The two major peaks at 0.0236 and 0.0205 Å^{-1} correspond to "wavelength" components in the optimal potential that are one-half the de Broglie wavelengths of electrons with incident energies 0.011 and 0.013 eV, respectively, passing over a constant potential region of 0.005 eV.

is quite good. Figure 6(c) plots $R(E)$ using the initial guess potential; note the dramatic difference between this and $R(E)$ in Fig. 6(b) using the optimal potential, even though the magnitudes of the potentials do not differ by more than 0.0015 eV. As in Fig. 5(a), there is a characteristic "wavelength" associated with the optimal potential, although here it is slightly more complicated due to the more demanding objective. However, as in the previous case, the "wavelength" of this potential is roughly one-half of the de Broglie wavelength of electrons corresponding to incident energies in the range of 0.01–0.014 eV, i.e., the range of the target incident energies, passing over a constant potential of 0.005 eV.

One serious drawback of the optimal potential characteristic "wavelength" which is one half the electron de Broglie wavelength is that, as one goes to higher incident energies where better coherent transport is possible, the optimal potential structure will possess a higher structural resolution. From the perspective of fabrication, the lower the device resolution the better, and in many cases there will be a limit to the structural resolution that one can build, especially in the case of lateral heterostructures. In order to comply with these demands, we use an alternative gradient-filtering optimization procedure.[9] Here we use the same objective reflection $R'(E)$ and initial guess potential as in the previous case but restrict the "bandwidth" of the optimal potential so that it will not contain "wavelength" components smaller than 1000 Å. This is accomplished by removing the unwanted high-frequency components from the gradient at each iteration (see Ref. 9 for details). Figure 7(a) displays the optimal potential. Note that to compensate for the resolution restriction the magnitude of the potential increases from the last case. As expected, the achieved reflection coefficients do not match their objective values as closely as in the previous case without any filtering [compare Figs. 7(b) and 6(b)], but they are still a vast improvement over those obtained using the initial guess potential [Fig. 6(c)].

Finally we examine the case where $R'(E)$ is two narrow Gaussian functions centered at 0.011 and 0.013 eV. Figure 8(a) displays the optimal potential and Fig. 8(b) shows the resulting reflection coefficients $R(E)$ (solid line) superimposed on the objective reflection coefficients $R'(E)$. No restriction on the potential form was imposed here. Note that there is an overall slow "beat" in the potential; this can be explained by examining the "power spectrum" of the optimal potential in Fig. 8(c). In particular, note the two peaks at 0.0236 and 0.0205 Å^{-1} which correspond to the two "wavelengths" 266 and 306 Å, respectively. In line with the previous examples, these two "wavelengths" are one-half of the electron de Broglie wavelength at incident energies of 0.011 and 0.013 eV passing over a constant potential of 0.005 eV. The slow "beat" here is simply the difference between these two major components in the potential, i.e., it possesses a "frequency" of $0.0236-0.0205=0.0031$ Å^{-1}.

IV. CONCLUSIONS

In this paper we have demonstrated that a high degree of control of electron plane-wave reflection amplitudes through manipulation of the scattering potential is possible. Provided one has complete freedom in designing the scattering potential, one can achieve a wide range of reflection-coefficient objectives through delicate manipulation of the quantum interference effects. In the Appendix an algorithm is presented which will, given an initial wave packet and a final time τ, provide all possible final wave packets that could be created provided one has complete freedom in choosing the potential form. The method also yields the potential which will create a desired wave packet. The practical obstruction to this algorithm, however, is that in the process one has to solve several equations, which are transcendental in general, symbolically. The results presented in this paper should be viewed as a first step towards the goal of wave-packet "encoding," i.e., the coherent control of the wave-packet structure through optimal design of the scattering potential. Ultimately, the "encoding" process will be viewed in a time-dependent manner, where the initial incoming wave packet is scattered by the optimal potential and the desired outgoing wave packet is produced. Such an approach would allow for the manipulation of both the amplitude and the phase of the wave-packet Fourier components, thereby providing greater design versatility.

In this work we have neglected deleterious effects present in real solid-state devices such as lattice imperfections and phonons. These will adversely affect the ballistic transport properties and should be accounted for in more realistic designs. However, existing ultra-high-mobility two-dimensional electron systems have demonstrated ballistic ranges exceeding 10 μm at liquid-helium temperatures.[1,2] Therefore, the design methodology presented here is applicable to real systems. It should be noted that the general optimal control can be expanded to incorporate the effects of undesired scattering.

Finally, we reiterate that the major obstacle to overcome in order to implement the ideas presented here in the laboratory is the required structural resolution of the solid-generated potentials. The optimal potential structures presented here call for devices with resolutions of one-half the de Broglie wavelength of the incident electron in order to achieve maximum control. At present, this fine resolution is not possible in lateral heterostructures, and future work must therefore incorporate fabrication limitations into the theoretical design process. However, resolution on this scale is feasible for vertical structures.

ACKNOWLEDGMENT

This work is supported by the Army Research Office.

APPENDIX

In what follows, we will examine the question of the existence and the synthesis of an external potential $V(x)$ which will enable one to produce a desired wave packet at a prescribed final time τ, given that the primitive wave packet traverses this potential.

Let $\psi_{\text{in}}(x)$ be the primitive wave packet and let $\psi_{\text{out}}(x)$ be the desired wave packet at time τ. We expand both with respect to an eigenbasis of some operator of interest.

The choice of the operator of interest will depend on how the external potential (if one exists) is to be implemented. One appropriate choice is the position operator. Next, we truncate this eigenbasis to a finite number (N) of eigenfunctions of interest. Thus, for instance, if the position operator is the operator of choice, then these N eigenfunctions would be δ functions centered at some suitably chosen N points on a grid. Another natural choice is the eigenbasis consisting of eigenfunctions of the momentum operator. Of course, the choice of the operator should not influence the existence (or nonexistence) of the "designer" potential $V(x)$.

Suppose, therefore, that the expansion of the above two wave packets with respect to this finite eigenbasis $\psi_1,\ldots,\psi_N$ can be expressed as:

$$\psi_{\text{in}}(x)=\sum_{l=1}^{N} a^{l}_{\text{in}}\psi_l(x) ,$$

and

$$\psi_{\text{out}}(x)=\sum_{l=1}^{N} a^{l}_{\text{out}}\psi_l(x) .$$

Clearly then the vectors $\vec{a}_{\text{in}}=(a^1_{\text{in}},\ldots,a^N_{\text{in}})^t$ and $\vec{a}_{\text{out}}=(a^1_{\text{out}},\ldots,a^N_{\text{out}})^t$, being probability amplitudes, lie on the $2N-1$ dimensional sphere. We will utilize this fact to examine the existence of $V(x)$ in the following steps.

(1) Show that there is always a unitary matrix which transforms $\vec{a}_{\text{in}}$ to produce $\vec{a}_{\text{out}}$.

(2) Obtain an explicit expression for the most general such unitary matrix.

(3) Find the functional form of the logarithm of the unitary matrix in the above step. This logarithm is guaranteed to be a skew-Hermitian matrix.

(4) Divide the skew-Hermitian matrix in the preceding step by $i/\hbar$ and subtract from it the (Hermitian) matrix representation of the internal Hamiltonian.

(5) Examine when the Hermitian matrix obtained in the penultimate step can be expressed as (the matrix representation of) a local spatial potential.

We now carry out each of the above steps in greater detail. Before doing so, however, we mention that steps (1)–(3) can be succinctly stated using notions from the theory of smooth actions of Lie transformation groups. More precisely, steps (1)–(3) amount to stating that the group of order N unitary matrices, denoted $U(N)$, acts transitively on the $2N-1$ sphere with isotropy $U(N-1)$. However, to state things in such a fashion says nothing about the constructive aspects of the aforementioned recipe, which is what is required by us. We now resume our analysis of the various steps involved in the construction of the putative potential.

(1) We construct the unitary matrix U which takes $\vec{a}_{\text{in}}$ to $\vec{a}_{\text{out}}$ as the product of two unitary matrices $U_2U_1^{\dagger}$ (thereby ensuring that U is unitary too), with $U_1^{\dagger}$ denoting the conjugate transpose of some unitary matrix U_1 (thereby rendering $U_1^{\dagger}$ unitary also). To that end we first denote the vector $(1,0,\ldots,0)^t$ by v_p which clearly lies on the $(2N-1)$-dimensional sphere. The matrix U_1 is formed in the following fashion. Let the first column of U_1 be the vector $\vec{a}_{\text{in}}$, and the remaining columns be any choice of unit norm vectors in C^N which, together with $\vec{a}_{\text{in}}$, form an orthonormal basis for C^N. Two observations are to be noted. (i) U_1 is a unitary matrix. Indeed, any nonsingular matrix whose columns (or rows) form an orthonormal basis for C^N is unitary (and vice versa). (ii) $U_1v_p=\vec{a}_{\text{in}}$. Therefore, it follows that $v_p=U_1^{-1}\vec{a}_{\text{in}}$. But U_1, being unitary, satisfies $U_1^{-1}=U_1^{\dagger}$, and this latter matrix is (by the properties of unitary matrices) also unitary. As for U_2, it is constructed in exactly the same manner as U_1, with the difference that in its construction we replace $\vec{a}_{\text{in}}$ everywhere by $\vec{a}_{\text{out}}$. We thus have that $U_2v_p=\vec{a}_{\text{out}}$, and therefore $U_2U_1^{\dagger}\vec{a}_{\text{in}}=\vec{a}_{\text{out}}$, as claimed.

(2) It is apparent that the unitary matrix U in the step above is not the only unitary matrix which will yield $\vec{a}_{\text{out}}$ upon multiplying $\vec{a}_{\text{in}}$. To analyze the degree of indeterminacy in the matrix U we first note that if V and W are two matrices which yield $\vec{a}_{\text{out}}$ when multiplying $\vec{a}_{\text{in}}$, then the matrix $V^{\dagger}W$ fixes the vector $\vec{a}_{\text{in}}$, i.e., $V^{\dagger}W\vec{a}_{\text{in}}=\vec{a}_{\text{in}}$ (we will adopt the expression "fixes" to mean this last equation). Likewise, $WV^{\dagger}$ fixes $\vec{a}_{\text{out}}$. Thus the most general unitary matrix which produces the vector $\vec{a}_{\text{out}}$ from $\vec{a}_{\text{in}}$ is of the form NUL, where N is any unitary matrix which fixes $\vec{a}_{\text{out}}$, L is any unitary matrix which fixes $\vec{a}_{\text{in}}$, and U, of course, is the unitary matrix constructed in the step prior to the present one. Thus, it remains to examine which unitary matrices fix the vectors $\vec{a}_{\text{in}}$ and $\vec{a}_{\text{out}}$. For this, it is convenient to determine the unitary matrices which fix the vector v_p. Clearly, by the special structure of the vector v_p, the only such matrices are $N\times N$ unitary matrices with both the first row and the first column equal to the vector v_p itself, and with the other elements constituting any arbitrary $(N-1)\times(N-1)$ unitary matrix. We will denote a typical such matrix by Λ. Now clearly all matrixes admitting an expression of the type $U_1\Lambda U_1^{\dagger}$ leave $\vec{a}_{\text{in}}$ fixed. Conversely, one can show that any unitary matrix which fixes the vector $\vec{a}_{\text{in}}$ necessarily admits such an expression. Indeed, if V be any such unitary matrix, then the unitary matrix $U_1^{\dagger}VU_1$ leaves v_p fixed and hence must be of the form described above. Consequently, $U_1^{\dagger}VU_1=\Lambda$. Thus V equals $U_1\Lambda U_1^{\dagger}$. By the same reasoning every unitary matrix which fixes $\vec{a}_{\text{out}}$ can be written as $U_2\Delta U_2^{\dagger}$, where Δ is any unitary matrix which leaves v_p fixed. One can easily show that the matrices which leave v_p fixed form a group [which is, in fact, isomorphic to $U(N-1)$]. Therefore, $\Delta\Lambda$ is also a unitary matrix which fixes v_p. In order to avoid introducing too many new symbols, we will denote this matrix also by Λ. Therefore, putting all of the foregoing analysis together, one concludes that all matrices (and only they) expressible as $U_2\Lambda U_1^{\dagger}=\hat{U}$ take $\vec{a}_{\text{in}}$ to the vector $\vec{a}_{\text{out}}$.

(3) The next step is to find the logarithm of the unitary matrix $\hat{U}$ obtained in step (2). It is a standard fact that the logarithm of a unitary matrix is skew Hermitian. To find the logarithm explicitly we first diagonalize the unitary matrix. The diagonalizing matrix may also be taken to be unitary. Since the eigenvalues of a unitary matrix are all of the form $\exp(i\gamma_k), k=1,\ldots,n$, we obtain

$$\hat{U}=P\,\text{diag}(e^{i\gamma_k})P^{\dagger} ,$$

with P being the (unitary) matrix which diagonalizes $\hat{U}$. We define the logarithm of $\hat{U}$ to be the matrix $\hat{S}$ defined as $P\Gamma P^{\dagger}$, where Γ is a diagonal matrix with diagonal entries $i\gamma_k, k=1,\ldots,n$. One can verify that $\exp(\hat{S})=\hat{U}$. Hence the matrix $\hat{T}=(\hbar\hat{S})/(i\tau)$ is Hermitian, a fact which will be used in the step immediately below.

(4) We want $\exp[i(H_{\text{int}}+H_{\text{ext}})\tau/\hbar]$ to equal the desired unitary matrix $\hat{U}$. Here, τ is the final time, the matrix representation of the internal Hamiltonian is denoted by H_{int}, and that of the external or interaction Hamiltonian is denoted as H_{ext}. Both these Hamiltonians are assumed to be time independent. If we subtract from $\hat{T}$ (with $\hat{T}$ given by the preceding step) the Hermitian matrix H_{int}, we get another Hermitian matrix. Now any Hermitian operator represents a valid quantum-mechanical perturbation operator. However, not every quantum-mechanical perturbation operator is a local spatial potential operator.

(5) Further conditions are needed to render the perturbation operator of the preceding step a local spatial potential. Let us analyze these additional conditions, assuming that the eigenbasis chosen consists of eigenfunctions of the position operator. The analysis for other bases is the same, and the existence of a potential operator ought not to depend on the choice of the eigenfunctions. Eigenfunctions of the position operator have been chosen since, in practice, one of the most common techniques for constructing a local potential consists of prescribing its putative values over a finite grid of points. The matrix representation of the putative potential, H_{ext}, is diagonal, with diagonal elements being precisely the values of the potential at the points of the chosen grid. The matrix representation of the internal Hamiltonian need not be diagonal but is certain to be Hermitian. For instance, if the internal Hamiltonian is the kinetic energy of a free electron, one can obtain its matrix representation by inverting the fast Fourier transform (e.g., see Ref. 10). If H_{ext} is to be a spatial potential, it is clear that a necessary and sufficient condition is that the off-diagonal elements of $\hat{T}$ and H_{int} should be the same. Before examining this stipulation any further, we first note that if it is met then the diagonal elements of H_{ext} will automatically be real, since they are the differences of the corresponding diagonal elements of $\hat{T}$ and the matrix H_{int}, both of which are Hermitian and are thus guaranteed to have real diagonal elements.

It is, in general, difficult to characterize situations under which the diagonal elements of $\hat{T}$ and H_{int} will be the same in a succinct fashion. What one can do, however, is to carry out a dimension count to examine the restrictions that one must place on ψ_{out} for the existence of a potential. The number of independent, off-diagonal elements is N^2-N. This is because a Hermitian matrix, with complex entries, has a total of N^2 real independent elements, of which N are diagonal elements. We have, therefore, N^2-N real equations to be satisfied. Let us now examine the number of free parameters available to us. Recall that the unitary matrix $\hat{U}$ has an arbitrary factor of $(N-1)\times(N-1)$ unitary Λ in it. Now the number of independent real parameters in such a unitary matrix is $(N-1)^2$. This follows because unitary matrices form a Lie group and their dimension is the same as that of their Lie algebra, the Lie algebra of skew-Hermitian matrices, and the latter has the above dimension since $N^2-N-(N-1)^2=N-1$. Hence, we will require $N-1$ more real parameters which are free. This will limit the choices of the vector ψ_{out}. Recall that ψ_{out} appears in $\hat{U}$ (explicitly) since it appears explicitly in the unitary matrix U_2, which is one of the multiplicative factors in the "designer" unitary matrix. Now ψ_{out} consists of N complex numbers (thus $2N$ real numbers) with one constraint. Thus it provides one with $(2N-1)$ free parameters, out of which we need $N-1$, thus leaving a total of N parameters which can be prescribed *a priori*. This then gives us the possible choices for the final wave packet. We emphasize that this is only a dimension argument. Not all real equations have real solutions, and when they do these need not be unique. Furthermore, in practice, one will be usually forced to impose further restrictions on H_{ext}. The upshot of the foregoing analysis is that even without any practical restrictions on the potential form one cannot synthesize any desired wave packet via a local spatial potential. In the parlance of control theory, the problem of synthesizing a desired wave packet starting from a given primitive wave packet, via an external local spatial potential, is not controllable. However, in principle, one can via the preceding recipe determine the final wave packets which *can* be produced from a given primitive wave packet through the use of an artificial local spatial potential. In the language of control theory, we can determine the reachable set from a given primitive wave packet. We remark, however, that the problem under consideration here is not of the type studied traditionally in control theory, because our external control, namely the local spatial potential, is not time varying, as is the case for traditional applications of control theory.

[1]C. W. Beenakker and H. van Houten, Solid State Phys. **44**, 1 (1991).

[2]For recent results, see, e.g., *Proceedings of the 10th International Conference on Electronic Properties of Two-Dimensional Systems, Newport, RI, May–June 1993,* Surf. Sci. (to be published).

[3]G. N. Henderson, T. K. Gaylord, and E. N. Glytsis, Phys. Rev. B **45**, 8404 (1992).

[4]C. D. Schwieters and H. Rabitz, Phys. Rev. A **44**, 5224 (1991); S. Shi and H. Rabitz, Comput. Phys. Commun. **63**, 71 (1991).

[5]E. Merzbacher, *Quantum Mechanics* (Wiley, New York, 1970).

[6]S. E. Koonin, *Computational Physics* (Benjamin/Cummings, Menlo Park, 1986).

[7]S. Shi and H. Rabitz, J. Chem. Phys. **92**, 364 (1990).

[8]C. Kittel, *Introduction to Solid State Physics* (Wiley, New York, 1986).

[9]P. Gross, D. Neuhauser, and H. Rabitz, J. Chem. Phys. **96**, 2834 (1992).

[10]C. C. Marston and G. G. Balint-Kurti, J. Chem. Phys. **91**, 3571 (1989).